Journal of Materials Chemistry

Cite this: J. Mater. Chem., 2012, 22, 21727

www.rsc.org/materials

PAPER

A facile and low-cost synthesis of promising absorber materials on $Cu_2ZnSn(S_x,Se_{1-x})_4$ nanocrystals consisting of earth abundant elements with tunable band gap characteristics

Seung Wook Shin,[a] Jun Hee Han,[a] Yeon Chan Park,[b] G. L. Agawane,[b] Chae Hwan Jeong,[c] Jae Ho Yun,[d] A. V. Moholkar,[e] Jeong Yong Lee[f] and Jin Hyeok Kim[g]

Received 13th June 2012, Accepted 3rd August 2012
DOI: 10.1039/c2jm33802e

In this paper, we report a facile, low cost synthesis and characterization of kesterite $Cu_2ZnSn(S_x,Se_{1-x})_4$ (CZTSSe) nanocrystals (NCs) by a two-step process involving a solution-based precursor and a post-annealing route. The effects of different Se vaporization temperatures, ranging from 350 °C to 550 °C, on the structural, chemical, compositional, and optical properties of CZTSSe NCs were investigated. X-ray diffraction patterns, Raman spectroscopy, and transmission electron microscopy results indicated that the precursor powder showed several broad peaks that could not be assigned to Cu_2ZnSnS_4 (CZTS), ZnS, $Cu_{2-x}S$, Sn_2S_3 and Cu_2SnS_3. However, the post-annealed NCs with and without Se vaporization were a single kesterite CZTS phase without a secondary phase. UV-vis spectroscopy results showed that the absorption coefficients of all the post-annealed NCs were over 10^4 cm^{-1} in the visible region, and the optical band gap energy decreased systematically from 1.46 eV to 1.14 eV with increasing Se vaporization temperatures.

Recently, kesterites $Cu_2ZnSn(S_x,Se_{1-x})_4$ (CZTSSe) have attracted interest as promising In- and Ga-free absorber materials for photovoltaic applications due to their direct band gap energy of 1.5 eV, high absorption coefficient of $>10^4$ cm^{-1} in the visible wavelength region, and high availability in nature, which are superior when considering drawbacks encountered in CdTe- and $Cu(In, Ga)Se_2$ (CIGS)-based thin film solar cells (TFSCs).[1–3] In addition, W. Ki and H. W. Hillhouse have shown the maximum efficiency for single junction Cu_2ZnSnS_4 TFSC devices (CZTS, $\eta = 32.4\%$, $V_{oc} = 1.21$ V, $J_{sc} = 29.6$ mA cm^{-2} and FF = 89.9%) and $Cu_2ZnSnSe_4$ (CZTSe, $\eta = 31.0\%$, $V_{oc} = 0.71$ V, $J_{sc} = 51.4$ mA cm^{-2} and FF = 84.8%) using photon balance calculations (Shockley–Queisser style detailed balances).[4] Although the CZTSSe-based TFSCs showed higher theoretical efficiency than that of CdTe and CIGS, the practical power conversion efficiency (PCE), approximately 10%, was achieved using the CZTSSe absorber layer.[1] Many research groups have studied the synthesis of CZTSSe thin films, and the fabrication of CZTSSe-based TFSCs, using a variety of physical and chemical techniques.[1] The literature survey for CZTSSe-based TFSCs indicates that a record efficiency of 10.1% has been achieved, using a solution-based hybrid slurry process, while vacuum-based processes obtained a lower efficiency of 8.4% using the thin CZTS absorber layer (~600 nm) by sulfurization of the thermally evaporated precursors.[2,3] In addition, the high vacuum physical techniques have several drawbacks, including high cost, vacuum requirement, temperature dependence, complicated apparatus, and most importantly the formation of unwanted phases during deposition processes.[5–8] The industrial throughput of TFSC devices is limited in meeting the energy demand of mankind throughout the globe.[9] Therefore, many researchers have studied a solution-based approach, owing to a low-cost and simple process, which includes spin coating, drop casting, doctor blade deposition, spray pyrolysis, sol–gel and electro- and photo-chemical deposition, in order to solve these drawbacks and improve the power conversion efficiency of the present TFSCs.[1,10] J. J. Scragg *et al.* reported 3.2% of CZTS-based TFSCs using the sulfurization of electrodeposited Cu/Sn/Cu/Zn stacked elemental precursor thin films.[11] In this research, the uniformity and morphology of metallic stacked precursor thin

[a]*Department of Materials Science and Engineering, KAIST, Daejeon 305-701, South Korea*
[b]*Photonics Technology Research Institute, Department of Materials Science and Engineering, Chonnam National University, 300 Yongbong-Dong, Puk-Gu, Gwangju 500-757, South Korea*
[c]*Solar city center, Development of Advanced Components & Materials, Korea Institute of Industrial Technology, Gwangju, 500-480, South Korea*
[d]*Photovoltaic Research Group, Korea Institute of Energy Research, 71-2 Jang-Dong Yuseong-Gu, Daejeon 305-343, South Korea*
[e]*Department of Physics, Shivaji University, Kolhapur 416-004, India*
[f]*Photonics Technology Research Institute, Department of Materials Science and Engineering, Chonnam National University, 300 Yongbong-Dong, Buk-Gu, Gwangju 500-757, South Korea. E-mail: jinhyeok@chonnam.ac.kr; Fax: +82-62-530-1699; Tel: +82-62-530-1709*
[g]*Department of Materials Science and Engineering, Korea Advanced Institute of Science and Technology, 335 Gwahangno, Yuseong-gu, Daejeon 305-701, South Korea. E-mail: j.y.lee@kaist.ac.kr; Fax: +82-42-350-3310; Tel: +82-42-350-4216*

films were improved by introducing a rotating disc electrode system. Recently, D. A. R. Barkhouse *et al.* have reported the best conversion efficiency of 10.1% for CZTSSe-based TFSCs using the hybrid solution–particle approach.[2] Although the CZTS-based TFSCs, using the non-vacuum approach, have several merits and the highest efficiency record, they are limited by various problems, such as the incorporation of undesired impurities (carbon, oxygen, binder reminder, and solvent) and chemical toxicity (*e.g.* hydrazine hydrate) for scaling up massive TFSCs production, which needs to be addressed.[1,4,12,13] Recently, nanocrystal (NC)-based absorber thin films from solution synthesis routes such as solvothermal, low temperature colloidal, and the hot injection method have been found to be particularly attractive for large-scale manufacturing due to low manufacturing costs and the possibility of large scale and high throughput using roll to roll TFSC fabrication processes.[1] C. Steinhagen *et al.* reported that the CZTS NCs can be synthesized by a solvothermal method, at a temperature of 280 °C, for 1 hour, using oleylamine and hexadecylamine as stabilizers.[14] The characteristics of CZTS-based TFSCs showed a very low efficiency of 0.23%. Guo *et al.* reported the synthesis of CZTSSe and CZTSe NCs by a hot injection solution method at a temperature over 225 °C.[15] Oleylamine or hexadecylamine has been used to stabilize the NCs in organic solvents. The CZTS-based TFSCs have been achieved at an efficiency of 0.8% (0.12 cm^2), using an Al/ITO/i-ZnO/CdS/CZTS/Mo/glass multi-stacked structure. Further research on optimizing compositional ratios using the spin coating method has resulted in the PCE of 7.2%.[16] Although the shape and size of these CZTS NCs have been found to be uniform, hazardous chemicals, such as oleylamine and hexadecylamine, were required for the synthesis process. This issue has stimulated the research community to investigate the hazardous chemical-free solution-based process for the synthesis of CZTSSe NCs with adequate photovoltaic characteristics. To solve these problems, we have recently reported a facile and low-cost synthesis of CZTS NCs by sulfurization of microwave-assisted precursor powder without hazardous chemicals. The sulfurized precursor powders were successfully synthesized as a single kesterite CZTS structure, without a secondary phase, yielding a grain size of ~42 nm and a direct band gap energy of 1.46 eV.[12] The optical band gap energy of CZTSSe absorber thin films is strongly related to the PCE of CZTSSe-based TFSCs.[1,17] The previous literature surveys indicated the higher PCE of CZTSSe-based TFSCs with a relatively narrow band gap energy of 1.1–1.2 eV compared to that with a band gap energy of 1.5 eV.[2] Therefore, band gap engineering of CZTSSe absorber materials was required in order to improve the PCE. Few reports on the band gap engineering of CZTSSe absorber materials, using Se or Ge in the CZTS, are included; M. Danilson and J. He *et al.* reported the band gap engineering of CZTSSe absorber powder by introducing Se binary compounds into the sintering process, and the band gap energy of CZTSSe decreased from 1.5 eV to 0.95 eV with the decreasing content of Se binary compounds.[18,19] G. M. Ford *et al.* reported the synthesis of $Cu_2Zn(Sn_{1-x}Ge_x)S_4$ (CZTGS) NCs from a batch reaction in an oleylamine bath by the hot injection method.[20] The band gap energy of CZTGS NCs increased from 1.5 eV to 2 eV, and 6.8% PCE of CZTGS-based TFSCs has been achieved at a compositional ratio of Ge/(Ge + Sn) = 0.7 and a band gap energy of 1.94 eV. Although the above-mentioned research has confirmed the good engineering of CZTSSe-based absorber materials, more detailed research on band gap engineering, through the addition of Se in the CZTSSe absorber materials, is needed in order to improve the PCE of CZTSS-based TFSCs and to develop the low-cost synthesis process. In this paper, we report the synthesis and band gap engineering of CZTSSe NCs prepared using microwave-assisted precursor powders without hazardous chemicals; the effects of different Se vaporization temperatures on the structural, morphological, and optical properties of CZTS NCs were investigated.

Copper(II) acetate (Cu(OAc), 99.99%), zinc acetate (Zn(OAc), 99.99%), tin(IV) chloride ($SnCl_2$, 99.99%), thioacetamide (TAA, 99.99%) and Se pellets (99.99%) were purchased from Aldrich and were used as received. The precursor solution was prepared using 40 mL of 0.2 M Cu(OAc), 40 mL of 0.1 M Zn(OAc) and 40 mL of 0.1 M $SnCl_2$. Subsequently, 40 mL of a 0.2 M TAA solution was added, and the pH was adjusted to 7 by adding ammonia (NH_4OH) solution with constant magnetic stirring for 10 minutes at room temperature. During this step, the color of the precursor solution changed from transparent to brown-green. After stirring for 10 minutes, the precursor solution was irradiated with microwave energy, using a commercial microwave oven (KR-B200B, Daewoo, Korea), at 700 W for 10 minutes. In the first 6 minutes, the color of the precursor solution was not changed. After 6 minutes, the precursor solution started boiling and the color changed from brown-green to dark-blue. When the microwave assisted process was completed, the precursor solution was cooled to room temperature in air, and the resultant solution was a mixture of water and precursor nanocrystals (NCs). In order to separate the water from precursor NCs, the precursor solution was centrifuged at 3000 rpm for 10 minutes. This process was repeated three times. Finally, the precursor powder was dried in a vacuum oven at 60 °C for 8 hours. In order to improve crystallinity and selenization of CZTSSe NCs, the Se pellets and precursor powders were placed in the left and right zones, respectively, in a commercialized furnace system. After inserting Se powder and precursor powder into the furnace system, a vacuum of up to 10^{-3} mTorr was created using a pumping system and Ar gas was flowed at 50 sccm. The Se vaporization temperatures were varied from 350 °C to 550 °C at an interval of 50 °C for 1 hour, while the precursor powder temperature was fixed at 550 °C for 1 hour using a commercial furnace system. The heating and cooling rates were 10 °C min^{-1} and 5 °C min^{-1}, respectively. After the annealing process, they were cooled naturally for 4 hours. The annealed NCs were further used for their structural, compositional, chemical and optical characterizations. The crystallographic information of the NCs was obtained from powder X-ray diffraction (PXRD, PANalytical, X'Pert-PRO, the Netherlands) operated at 45 kV and 40 mA. The bright-field (BF) transmission electron microscopy (TEM) images, their corresponding selected area electron diffraction (SAED) patterns, and high-resolution (HR) TEM images of the NCs were obtained using a JEOL-3010 at an operating voltage of 300 kV. Elemental mapping images and energy-dispersive X-ray spectra were acquired by energy-dispersive X-ray spectroscopy (EDS), using a Tecnai G2 F30 installed in the scanning transmission electron microscope (STEM) equipped with a high-angle annular dark-field (HAADF) unit.

The simulated images of atomic arrangement were also obtained using the National Center for Electron Microscopy Simulation Software (NCEMSS) from the Lawrence Berkeley National Laboratory Institute. The compositional ratios of the NCs were analyzed by an EDS attached to the field emission scanning electron microscope (FE-SEM, JMS-7500F, JEOL, Japan). The chemical binding energy of the annealed NCs was examined using a high-resolution X-ray photoelectron spectroscope (HR-XPS, VG Multilab 2000, Thermo VG Scientific, UK) at room temperature. The binding energies were calibrated using the carbon 1s line at 285.0 eV. The optical absorption of the NCs was measured using a UV-visible spectroscope (Cary 100, Varian, Mulgrave, Australia) at room temperature.

The structure of CZTS is a tetragonal kesterite in which each cation is bonded to four sulfur anions and the cation layer alternates with the sulfur anion layer along the crystallographic *c*-direction, as CuZn/SS/CuSn/SS.[15] This structure is similar to the chalcopyrite structure of $CuInS_2$, in which the cation and anion layers alternate similarly to those in CuIn/SS/CuIn/SS.[15]

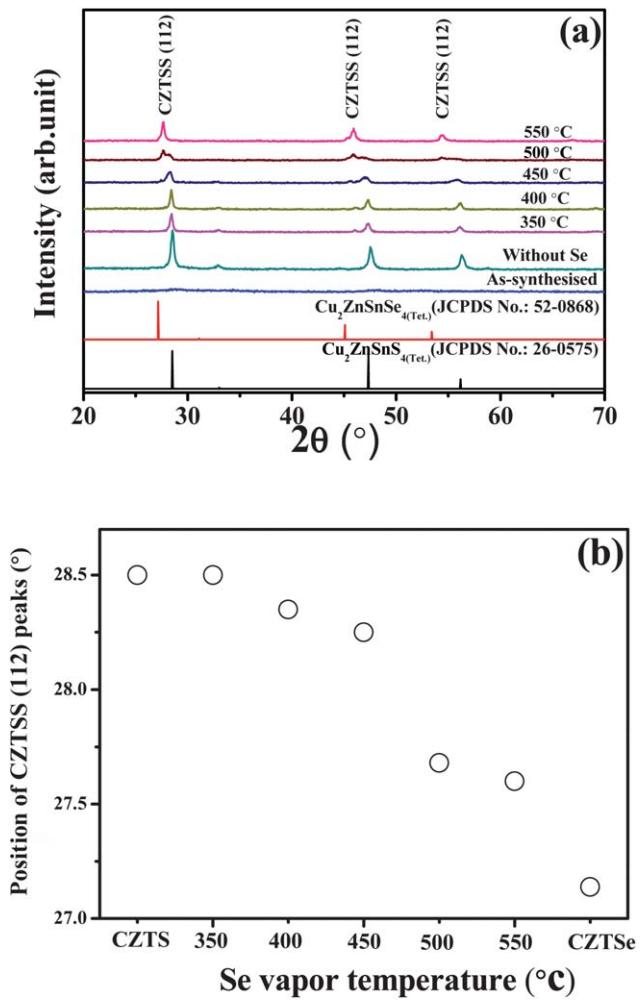

Fig. 1 PXRD patterns (a) and (112) peak position (b) of the microwave assisted precursor and post-annealed CZTSSe NCs at different Se vaporization temperatures. The peaks are indexed to the different planes according to the tetragonal CZTS (JCPDS no.: 26-0575) and tetragonal CZTSe (JCPDS no.: 89-4714), indicating that the three compounds have similar diffraction patterns.

Fig. 1 shows the powder X-ray diffraction (PXRD) patterns of the microwave-assisted precursor and post-annealed powder samples with and without different Se vaporization temperatures. The PXRD patterns of the microwave-assisted precursor powders showed weak peaks that could not be assigned to CZTS, ZnS, $Cu_{2-x}S$, SnS and Cu_2SnS_3 (CTS) phases (JCPDS no.: 26-0575 (CZTS/Tet.), 80-0020 (ZnS/Cub.), 89-2028 (SnS_2/Hex.) and 89-4714 (CTS/Tet.)). The post-annealed powders, with and without Se vaporization, showed strong diffraction peaks corresponding to the (112), (200), (220), (312), (224), (008) and (332) planes of a single kesterite-type CZTSSe structure. A shoulder observed to the left of the (112) plane for CZTS NCs without Se vaporization might have originated from stacking faults related to cation disordering, which are similar to faults observed in $CuInSe_2$ and CIGS.[15] The intensity of the (112) plane for CZTSSe NCs decreased with increasing Se vaporization temperature. The position of the CZTSSe (112) plane (Fig. 1(b)) of CZTS NCs systemically shifted towards a lower diffraction angle with increasing Se vaporization temperature. While increasing the Se vaporization temperature in the annealing process, the replacement of the S atoms by the large Se atoms increased, indicating an increase in the crystal lattice parameters of CZTSSe NCs because the ionic radius of Se^{2-} (0.198 nm) is larger than that of S^{2-} (0.184 nm).[2] The separated diffraction peaks were observed near 28.4° for CZTSSe NCs at Se vaporization temperatures of 450 °C and 500 °C. From the position of (112) peaks of CZTS and CZTSe, according to JCPDS data, these separated diffraction peaks confirmed the CZTS and CZTSe phase compounds in the CZTSS NCs. This characteristic suggested that the small portion of CZTS or CZTSe compounds can be synthesized on the CZTSSe NCs using the Se vaporization process.

Fig. 2 shows the BF-TEM images of post-annealed CZTS NCs without Se vaporization (a); (HR)-TEM image obtained from Fig. 2(a) (b), the magnified HR-TEM image of a CZTS NC in the small red square region in Fig. 2(b) (c); its simulated lattice image (d) under conditions of 30 Å thickness and 50 Å defocus; the fast-Fourier transform image of the square region in Fig. 2(b) (e) and the simulated lattice image of the diffraction pattern (f). There are many stacking faults in a CZTS NC (Fig. 2(a)), and these defects in CZTS NCs were found in the literature survey. Our previous work on TEM studies indicated that the average diameter of CZTS NCs is 42.1 ± 12.7 nm, with a wide grain size distribution of 30%. The magnified HR-TEM image of CZTS NCs showed that the atomic arrangement of the CZTS NCs, with *d*-spacing values of 0.31689 nm and 0.31714 nm, resulted from the (112) plane. The observed atomic *d*-spacing (Fig. 2(b)), atomic lattice image (Fig. 2(c)) and its diffraction patterns (Fig. 2(e)) were in agreement with the simulated lattice image (Fig. 2(d)) and diffraction patterns (Fig. 2(f)) obtained from the National Center for Electron microscopy Simulation Software. The TEM and simulation results confirmed that the post-annealed NCs have a kesterite phase without secondary phases.

Fig. 3 shows the BF-TEM images of post-annealed CZTSSe NCs prepared at a typical Se vaporization temperature of 550 °C (a); HR-TEM image obtained from Fig. 3(a) (b); the magnified HR-TEM image of a CZTSSe NC in the small red square region in Fig. 3(b) (c); its simulated lattice image (d) under conditions of 30 Å thickness and 50 Å defocus; fast-Fourier transform image of the square region in Fig. 3(b) (e); and the simulated lattice

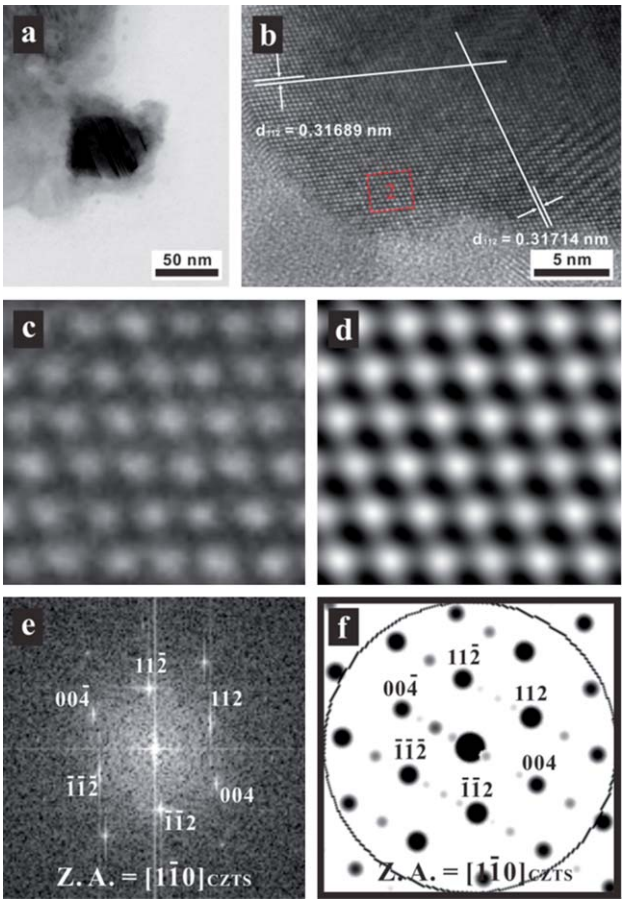

Fig. 2 BF-TEM images of post-annealed CZTS NCs without Se vaporization (a); (HR)-TEM image obtained from (a) (b); the magnified HR-TEM image of CZTS NCs in the small red square region in (b) (c); its simulated lattice image (d) under conditions of 30 Å thickness and 50 Å defocus; fast-Fourier transform image of the square region in (b) (e); and the simulated lattice image of the diffraction pattern (f).

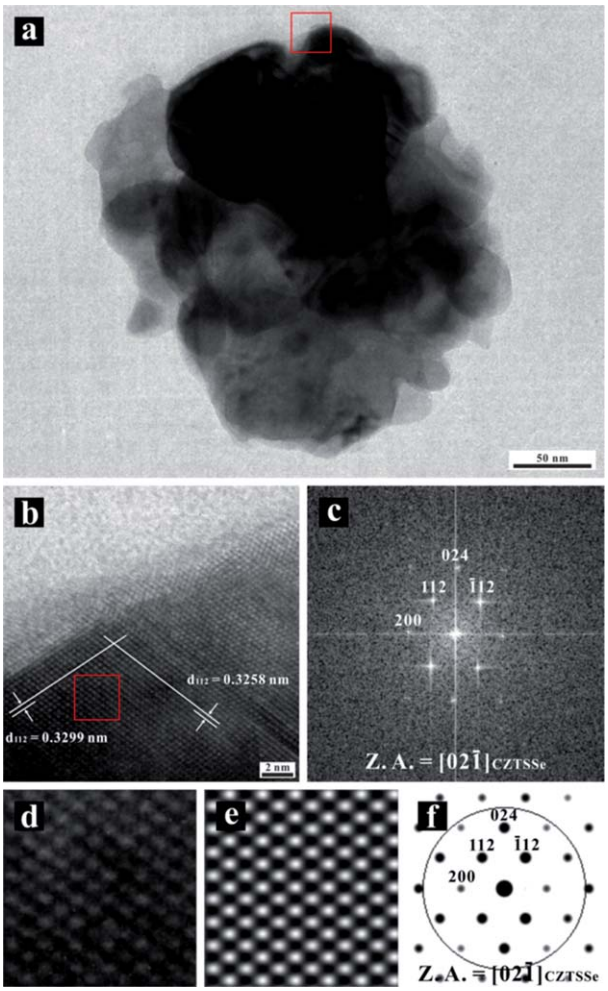

Fig. 3 BF-TEM images of post-annealed CZTSSe NCs at a Se vaporization temperature of 550 °C (a); HR-TEM image obtained from (a) (b); the magnified HR-TEM image of CZTSSe NC in the small red square region in (b) (c); its simulated lattice image (d) under conditions of 30 Å thickness and 50 Å defocus, fast-Fourier transform image of the square region in (b) (e); and the simulated lattice image of the diffraction pattern (f).

image of the diffraction pattern (f). The BF-TEM images of post-annealed CZTSSe NCs, formed at a Se vaporization temperature of 550 °C, indicated that the stacked faults of CZTSSe NCs were reduced compared with those of CZTSSe NCs formed without Se vaporization. These characteristics might be attributed to the better Se vapor-transport agent compared with S, which would have a more dramatic effect on grain growth.[17,21] The magnified HR-TEM image of CZTSSe NCs formed at a Se vaporization temperature of 550 °C showed atomic arrangement of the CZTSSe NC phase with *d*-spacing values of 0.3299 nm and 0.3258 nm, which were larger than those of CZTS NCs, formed without Se, and is matched with the (112) plane in the CZTSSe compounds. The phase/fast Fourier transform diffraction pattern (Fig. 3(c)) is also consistent with the peaks indexed to the zone axis of the [02$\bar{1}$] direction. The *d*-space value and diffraction patterns were in agreement with the simulated lattice image (Fig. 2(e)) and diffraction patterns (Fig. 2(f)). Thus, TEM observation and simulation results confirm that the NCs were of kesterite structure without secondary phases.

Fig. 4 shows the scanning transmission electron microscopy (STEM), energy-dispersive X-ray spectroscopy (EDS), and elemental mapping images of CZTSSe NCs using a Tecnia G2 F30 equipped with a high angle annular dark field (HAADP) (Fig. 3). The analysis showed that Cu, Zn, Sn, S, and Se were well-distributed in the NCs, without apparent element separation or aggregation. In addition, the EDS spectrum of the CZTSSe NCs (results are not shown here) showed five elements, including Cu, Zn, Sn, S and Se.

Fig. 5 shows the Raman spectra at room temperature (a) and the position of A_1 mode peaks (b) for post-annealed CZTSSe NCs formed at different Se vaporization temperatures. The A_1 modes were pure anion modes which correspond to vibrations of S and Se atoms surrounded by motionless neighboring atoms. The literature indicated that the A_1 mode of Raman peaks for CZTSe and CZTS were at approximately 196 cm^{-1} and 338 cm^{-1}, respectively.[22,23] Our Raman spectroscopy results also supported the shift at 338 cm^{-1} in A_1 mode for CZTSSe NCs. Only a very strong peak was observed, corresponding to a kesterite CZTS phase, whereas there were no Cu_2SnS_3 phase peaks located at 336 cm^{-1} or 351 cm^{-1} and the ZnS phase peaks were

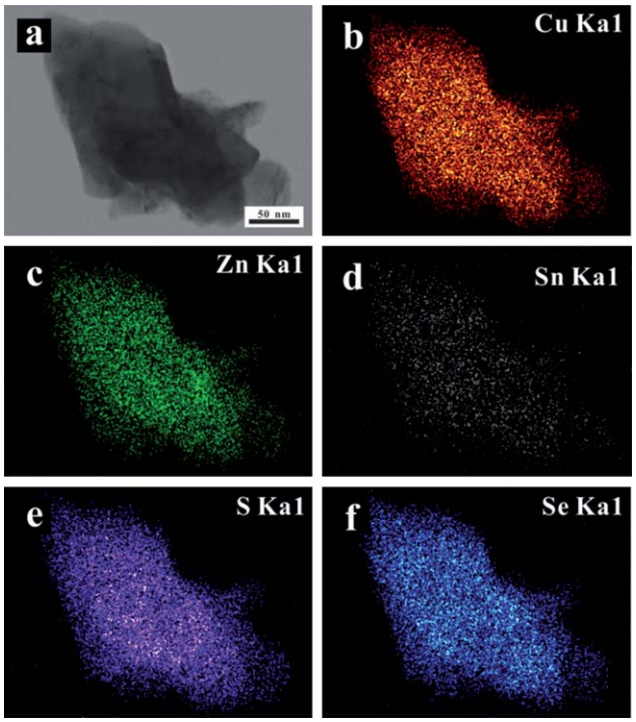

Fig. 4 HAADF-STEM image and elemental mapping images of CZTSSe NCs at a Se vaporization temperature of 550 °C. The images were obtained on carbon film-assisted Ni grids (200 mesh, Electron Microscopy Sciences) using a Tecnia G2 F30 equipped with a high-angle annular dark-field (HAADF) unit at an accelerating voltage of 300 kV.

located at 348 cm^{-1} (cubic phase) and 356 cm^{-1} (hexagonal phase), respectively.[23] In addition, several weak peaks located at 167 cm^{-1}, 252 cm^{-1}, 288 cm^{-1} and 374 cm^{-1} were observed; these are known to result from a kesterite CZTS phase. The post-annealed NCs, formed at Se vaporization temperatures of 350 °C and 400 °C, revealed weak Raman peaks from the CZTSe compound. This characteristic can be attributed to the low concentration of Se vapor and high concentration of S in the annealing atmosphere, which was created with the small portion of CZTSe and high portion of CZTS compounds.[17,21] Furthermore the post-annealed NCs, formed above the Se vaporization temperature of 450 °C, showed very strong peaks located from 219 cm^{-1} to 203 cm^{-1} which corresponded to a kesterite CZTSe phase.[22] It was also observed that some weak peaks were located from 315 cm^{-1} to 330 cm^{-1}, originating from the CZTS structure. The position of A_1 mode peaks of post-annealed NCs decreased towards the low Raman shift with increasing Se vaporization temperature (Fig. 5(b)). These Raman characteristics with intermediate values exhibited bimodal behavior similar to that observed in $CuIn(S_{1-x},Se_x)$, with a linear combination of 332 cm^{-1} and 196 cm^{-1} peaks as well as some noticeable peak broadening and a slightly shifted peak position.[21]

Fig. 6 shows the compositional ratios for ((Cu/(Zn + Sn))/(S + Se)) and S/(S + Se) of CZTSSe NCs formed at different Se vaporization temperatures. The compositional ratio of CZTS NCs, without Se vaporization, indicated the slight Cu- and Zn-rich but slight S poor. The compositional ratio for ((Cu/(Zn + Sn))/(S + Se)) and S/(S + Se) of CZTSSe NCs decreased with increasing Se vaporization temperature. This behavior was

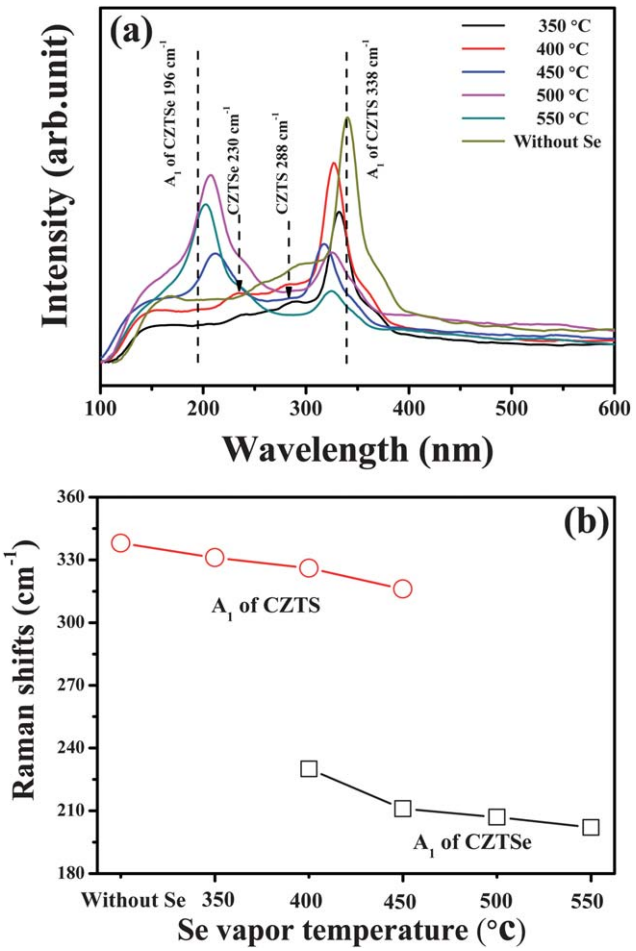

Fig. 5 Raman spectra (a) and position of A_1 mode peaks (b) for the CZTSSe NCs at different Se vaporization temperatures.

attributed to the low concentration of Se vapor and high concentration of S in the annealing atmosphere.

Fig. 7 shows the optical absorption coefficient (a) and the plot of $(\alpha h\nu)^2$ *vs.* photon energy ($h\nu$) (b) of the post-annealed CZTSSe NCs formed at different Se vaporization temperatures. The

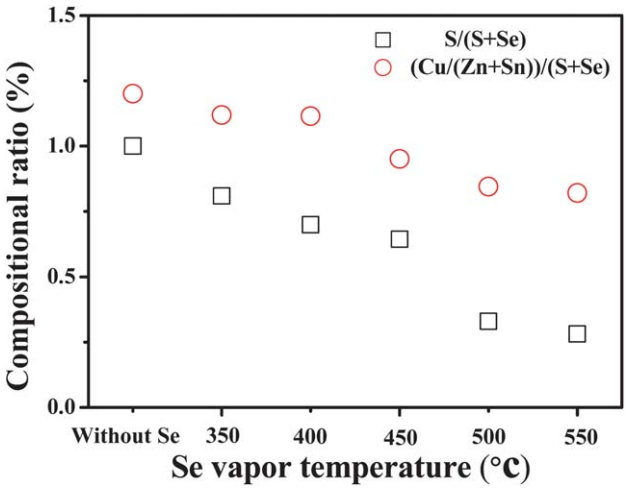

Fig. 6 Compositional ratio of CZTSSe NCs at different Se vaporization temperatures by EDS analysis.

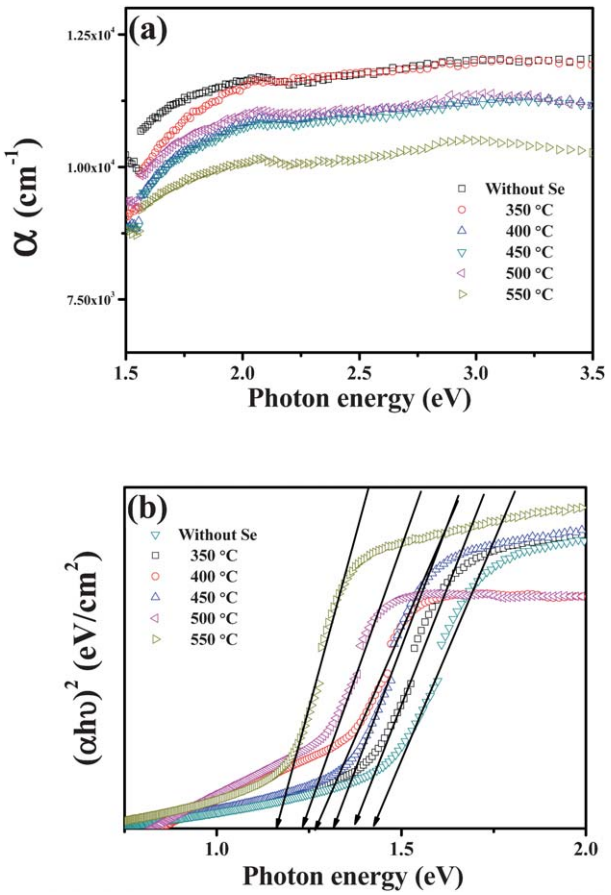

Fig. 7 Optical absorption coefficient (a) and plot of ($\alpha h\nu$) *vs.* photon energy ($h\nu$) of the CZTSSe NCs at different Se vaporization temperatures.

optical absorption coefficient of the post-annealed CZTSSe NCs was $>10^4$ cm^{-1} in the visible region, indicating a good absorption characteristic. The optical band gap energy (E_g) of the post-annealed CZTSSe NCs formed at different Se vaporization temperatures was measured by a linear extrapolation to the x-axis of the $(\alpha h\nu)^2$ *vs.* photon energy plot. The optical band gap energy of the post-annealed CZTS NCs formed without Se vaporization was 1.45 eV, indicating that this value was consistent with values reported in the literature: 1.45–1.6 eV. However, the optical band gap energy of the post-annealed CZTSSe formed with Se vaporization systemically decreased from 1.46 eV to 1.14 eV with increasing Se vaporization temperature. The narrow band gap energies of CZTSSe NCs with Se vaporization were attributed to the replacement of S atoms with Se ones. This tunable band gap characteristic was consistent with the literature on mono-grain CZTSSe powder and Cu(In,Ga)(S_{1-x},Se_x)$_2$ thin films. The above-mentioned results from XRD, TEM, Raman spectroscopy and UV-vis characterization techniques for CZTSSe NCs with tunable band gap energy indicated that these NCs have good absorption characteristics for photovoltaic applications.

Conclusions

CZTSSe NCs with tuneable band gap characteristic from 1.14 eV to 1.46 eV can be synthesized using a facile and simple route of microwave-assisted precursors, without involving hazardous chemicals for post-annealing, at different Se vaporization temperatures. XRD, TEM, Raman spectroscopy, and UV-vis spectroscopy results confirmed the kesterite type structure of the CZTSSe NCs. The STEM-EDS elemental mapping image revealed the presence of five elements in each individual NC. Studies on optimizing the synthesis processes and other parameters through precise control of the composition ratio of the CZTSSe NCs, along with the fabrication of CZTSSe-based TFSCs, are currently underway.

Acknowledgements

This work is supported by the Human Resources Development of the Korea Institute of Energy Technology Evaluation and Planning (KETEP) grant funded by the Korea government Ministry of Knowledge Economy and was funded partially by National Research Foundation of Korea (NRF) grant funded by the Korea government (MEST-no. 2011-0016564).

Notes and references

1 D. B. Mitzi, O. Gunawan, T. K. Todorov, K. Wang and S. Guha, *Sol. Energy Mater. Sol. Cells*, 2011, **95**, 1421.
2 D. A. R. Barkhouse, O. Gunawan, T. Gokmen, T. K. Todorov and D. B. Mitzi, *Prog. Photovoltaics*, 2012, **20**, 6.
3 B. H. Shin, O. Gunawan, Y. Zhu, N. A. Bojarczuk, S. J. Chey and S. Guha, *Prog. Photovolt: Res. Appl.*, 2011, **2**, 1174.
4 W. Ki and H. W. Hillhouse, *Adv. Energy Mater.*, 2011, **1**, 732.
5 W. Liu, D. B. Mitzi, M. Yuan, A. J. Kellock, S. J. Chey and O. Gunawan, *Chem. Mater.*, 2009, **22**, 1010.
6 Q. Guo, G. M. Ford, H. W. Hillhouse and R. Agrawal, *Nano Lett.*, 2009, **9**, 3060.
7 S. Ahn, C. Kim, J. H. Yun, J. Gwak, S. Jeong, B. H. Ryu and K. Yoon, *J. Phys. Chem. C*, 2010, **114**, 8108.
8 Q. Guo, S. J. Kim, M. Kar, W. N. Shafarman, R. W. Birkmire, E. A. Stach, R. Agrawal and H. W. Hillhouse, *Nano Lett.*, 2008, **8**, 2982.
9 D. B. Mitzi, *Adv. Mater.*, 2009, **21**, 3141.
10 H. Wang, *Int. J. Photoenergy*, 2011, **1**, 1.
11 J. J. Scragg, D. M. Berg and P. J. Dale, *J. Electroanal. Chem.*, 2010, **646**, 52.
12 S. W. Shin, J. H. Han, C. Y. Park, A. V. Moholkar, J. Y. Lee and J. H. Kim, *J. Alloys Compd.*, 2012, **516**, 96.
13 T. K. Todorov, K. B. Reuter and D. B. Mitzi, *Adv. Mater.*, 2010, **22**, E156.
14 C. Steinhagen, M. G. Panthani, V. Akhavan, B. Goodfellow, B. Koo and B. A. Korgel, *J. Am. Chem. Soc.*, 2009, **131**, 12554.
15 Q. Guo, H. W. Hillhouse and R. Agrawal, *J. Am. Chem. Soc.*, 2009, **131**, 11672.
16 Q. Guo, G. M. Ford, W. C. Yang, B. C. Walker, E. A. Stach, H. W. Hillhouse and R. Agrawal, *J. Am. Chem. Soc.*, 2010, **132**, 17384.
17 S. C. Riha, B. A. Parkinson and A. L. Prieto, *J. Am. Chem. Soc.*, 2011, **133**, 15272.
18 M. Danilson, M. Altosaar, M. Kauk, A. Katerski, J. Krustok and J. Raudoja, *Thin Solid Films*, 2011, **519**, 7407.
19 J. He, L. Sun, S. Chen, Y. Chen, P. Yang and J. Chu, *J. Alloys Compd.*, 2012, **511**, 129.
20 G. M. Ford, Q. Guo, R. Agrawal and H. W. Hillhouse, *Chem. Mater.*, 2011, **23**, 2626.
21 M. Y. Chiang, S. H. Chang, C. Y. Chen, F. W. Yuan and H. Y. Tuan, *J. Phys. Chem. C*, 2011, **115**, 1592.
22 D. Park, D. Nam, S. Jung, S. An, J. Gwak, K. Yoon, J. H. Yun and H. Cheong, *Thin Solid Films*, 2011, **519**, 7386.
23 S. W. Shin, S. M. Pawar, C. Y. Park, J. H. Yun, J. H. Moon, J. H. Kim and J. Y. Lee, *Sol. Energy Mater. Sol. Cells*, 2011, **95**, 3202.

